Research Article | Vol. 9, No. 3 | 1 Mar 2019 | OPTICAL MATERIALS EXPRESS 992
Optical Materials EXPRESS

Phase sensitive measurement of the wavelength dependence of the complex permittivity of a thin gold film using surface plasmon resonance

PETR HLUBINA,[1,*] MILENA LUNACKOVA,[2] AND DALIBOR CIPRIAN[1]

[1] *Department of Physics, Technical University Ostrava, 17. listopadu 15, 708 33 Ostrava-Poruba, Czech Republic*
[2] *Department of Mathematics and Descriptive Geometry, Technical University Ostrava, 17. listopadu 15, 708 33 Ostrava-Poruba, Czech Republic*
[*] *petr.hlubina@vsb.cz*

Abstract: We report on a new method for measuring the wavelength dependence of the complex permittivity of a thin gold film of a surface plasmon resonance (SPR) structure comprising a gold-coated SF10 slide with an adhesion film of chromium attached to an SF10 glass prism. The method is based on spectral interferometry and utilizes a setup with a birefringent crystal and the SPR structure in the Kretschmann configuration, in which channeled spectra are recorded and from them, the phase functions of the SPR for air at different angles of incidence are retrieved. The SPR phenomenon is manifested as an abrupt phase change with respect to the reference phase difference for the interference resolved with the SF10 glass prism alone. The phase changes for different angles of incidence are processed in the vicinity of the resonance wavelengths to obtain the real and imaginary parts of the complex permittivity in a wavelength range from 530 to 850 nm or equivalently, the parameters of a modified Drude-Lorentz model. This research, to the best of the authors' knowledge, is the first demonstration of spectral interferometry-based measurement of the complex permittivity function of a thin metal film, which is important from the point of view of material characterization directly performed in the Kretschmann configuration.

1. Introduction

It is well known that the performances of plasmonic devices are strongly influenced by the choice of metallic layers, whose optical constants or the complex permittivity functions affect the amplitude and the phase of the reflection coefficient at a metal-dielectric interface [1]. At these interfaces, the interaction of a *p*-polarized optical wave with free electrons leads at certain conditions to collective oscillations of electrons which are referred to as surface plasmons (SPs) and which affect a large number of physical or chemical responses. Because the SPs can be easily excited by the attenuated total reflection when the resonance condition is fulfilled [2–4], the effect of the surface plasmon resonance (SPR) has found a large number of applications in different research fields, including physics [2–4], chemistry [5], biology [6], etc.

A variety of SPR sensors have been proposed and confirmed [5, 7–14] which utilize extreme sensitivity of the SPR effect to refractive index changes of the surrounding medium at a metal-dielectric interface. In addition, because the resonance condition is accompanied by the amplitude and phase changes of reflected light wave, different physical quantities such the intensity [5], phase [7], resonant angle [8] or the resonant wavelength [9] can be measured to detect the SPR effect. Similarly, different experimental arrangements can be utilized so that the angular [10, 11] and wavelength interrogations [12–14] are possible.

The performance of the SPR sensor is strongly influenced by the choice of a thin metal film so it is crucial to know the complex permittivity function of the metal. Standard techniques to characterize thin metal films include spectral ellipsometry [15–17] and spectral reflectometry [18].

#352750 https://doi.org/10.1364/OME.9.000992
Journal © 2019 Received 23 Nov 2018; revised 27 Dec 2018; accepted 28 Dec 2018; published 5 Feb 2019

Optical Materials EXPRESS

Techniques of SPR-based spectral ellipsometry [19] and reflectometry [20–22] are also available. Recently, we proposed and realized a simple and cost-effective method compared to standard approaches like spectral ellipsometry, enabling to measure the wavelength dependence of the complex permittivity of a thin metal film [22]. Unfortunately, because this method is based on measuring the reflectance ratio for *p* and *s* polarizations, it is very sensitive to the birefringence properties of a read optical fiber. To overcome this limitation, we propose a phase sensitive measurement which has been utilized in our previous works [13, 23, 24].

In this paper, a new method for measuring the wavelength dependence of the complex permittivity of a thin gold film of an SPR structure is presented. The method is based on spectral interferometry and utilizes a setup with a birefringent crystal and the SPR structure in the Kretschmann configuration to record channeled spectra from which the phase functions of the SPR for air at different angles of incidence are retrieved. The SPR structure is represented by a gold coated SF10 slide with an adhesion film of chromium attached to an SF10 glass prism, and the SPR phenomenon is manifested by an abrupt phase change with respect to the reference phase difference resolved for the interference with the SF10 glass prism alone. The phase changes are processed in the vicinity of the resonance wavelengths to obtain the real and imaginary parts of the complex permittivity or equivalently, the parameters of the Drude-Lorentz model with two additional Lorentzian terms. This research, to the best of the authors' knowledge, is the first demonstration of spectral interferometry based measurement of the complex permittivity function of a thin metal film.

2. Experimental method

An experimental method used to measure the wavelength dependence of the complex permittivity of a thin gold film is based on spectral interferometry [13] and employs a setup shown in Fig. 1. Using white-light source WLS (halogen lamp HL-2000, Ocean Optics) with launching optics, an input optical fiber and collimating lens CL, a collimated beam of 1 mm diameter is generated which passes through linear polarizer P (LPVIS050, Thorlabs) oriented 45° with respect to the plane of incidence so that both *s*- and *p*-polarized components are present.

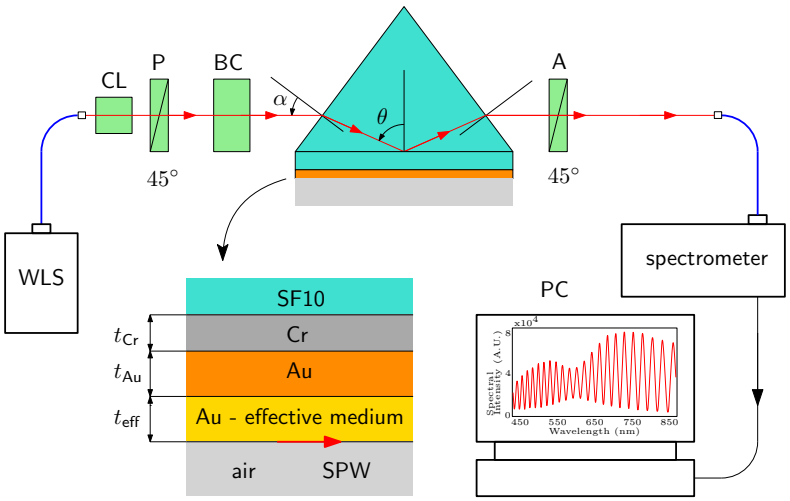

Fig. 1. Experimental setup for measuring the wavelength dependence of the complex permittivity of a thin gold film.

Next, these components pass through birefringent crystal BC in which they are mutually delayed to attain interference resolved by a spectrometer [13]. The thin gold film under study is

Optical Materials EXPRESS

part of an SPR structure in the Kretschmann configuration comprising a gold coated SF10 slide with an adhesion film of chromium coupled to a prism made of SF10 glass. When the light beam is incident on the SPR structure, both *s*- and *p*-polarized components undergo the amplitude and phase changes that are related to the complex reflection coefficients

$$r_{p,s}(\lambda) = \sqrt{R_{p,s}(\lambda)}\exp[\mathrm{i}\varphi_{p,s}(\lambda)], \tag{1}$$

where $R_{p,s}(\lambda)$ and $\varphi_{p,s}(\lambda)$ are the wavelength-dependent reflectances and phase changes on reflection for both polarizations. Because the *p*-polarized wave is subjected to the SPR phenomenon, both the reflectance ratio $R_p(\lambda)/R_s(\lambda)$ and the phase difference $\Delta(\lambda) = \varphi_p(\lambda) - \varphi_s(\lambda)$ are changed significantly near a resonance wavelength [24].

The reflected light passes through linear analyzer A (LPVIS050, Thorlabs) oriented 45° with respect to the plane of incidence so that *p*- or *s*-polarized components interfere and a channeled spectrum is resolved when the light is launched directly into a read optical fiber (M15L02, Thorlabs) of a spectrometer (USB4000, Ocean Optics). To retrieve the phase shift due to the SPR phenomenon from channeled spectra, the reference channeled spectrum needs to be recorded. It is obtained when the SF10 glass prism alone is used and the SPR phenomenon does not occur. The channeled spectrum can be represented in this case as [13]

$$I_{\mathrm{ref}}(\lambda) = I_{0\mathrm{ref}}(\lambda)\{1 + V_{\mathrm{ref}}(\lambda)\cos[\phi_{\mathrm{BC}}(\lambda) + \Delta_{\mathrm{ref}}(\lambda)]\}, \tag{2}$$

where $I_{0\mathrm{ref}}(\lambda)$ is the reference unmodulated spectrum, $V(\lambda)$ is a visibility term, $\phi_{\mathrm{BC}}(\lambda)$ is the phase difference (retardance) introduced by the birefringent crystal and $\Delta_{\mathrm{ref}}(\lambda)$ is the reference phase difference between the *p*- and *s*-polarized components.

Similarly, the channeled spectrum in the case when the SPR phenomenon occurs can be represented as

$$I(\lambda) = I_0(\lambda)\{1 + V(\lambda)\cos[\phi_{\mathrm{BC}}(\lambda) + \Delta(\lambda)]\}, \tag{3}$$

with quantities analogous to those in Eq. (2), but referring to the SPR phenomenon [13]. The corresponding phase shift, which can be retrieved from both channeled spectra, is given as

$$\delta(\lambda) = \Delta(\lambda) - \Delta_{\mathrm{ref}}(\lambda). \tag{4}$$

We prefer to consider, as in our previous work [22], the SPR phenomenon for air and to measure the wavelength dependence of the complex permittivity of a thin gold film via adjusting the resonance conditions at different angles of incidence. If the angle between the incident beam and the normal to the prism face (see Fig. 1) is denoted as α, the angle of incidence θ on the base of the equilateral prism is affected by the dispersion of both the prism glass and air, respectively [22].

The gold film under study is a part of the SPR structure comprising an SF10 glass slide substrate with an adhesion Cr film for the deposited Au film. The thickness of the chromium film is t_{Cr}=2 nm and the thickness of the gold film is 44.8 nm as specified by producer (Accurion, Germany). The surface morphology analysis has shown that the gold film is composed of homogenous and rough layers with thicknesses t_{Au}=42.8 nm and t_{eff}=2.0 nm, respectively, and that the volume fraction of the gold in the pseudolayer is q=0.5 [22]. To attach the SF10 glass slide with the deposited films to the equilateral prism (SF10 glass), a thin film of index-matching fluid (n_D=1.730, Cargille) was used.

3. Theoretical model

As the presented processing method is based on the fitting of the measured phase shift, the computation of the complex reflection coefficient of the layered SPR structure is an important

Optical Materials EXPRESS

task. Usually two methods are used. The first one is based on so called Airy's formula, where the reflection/transmission coefficient of a single layer is expressed using the reflection and transmission coefficients of layer boundaries and propagation through the layer (it can be derived using ray summation approach). Considering one-layer structure, these formulas are quite simple. In case of two or more layers, the one-layer formula can be used in a recursive manner. However, when the structure contains more then 3 layers, the computer implementation is more complicated and matrix formalism is preferred.

The matrix formulation of wave propagation in layered structures is based on continuity relations of electric and magnetic field tangential components across all boundaries of the thin film system, providing that the density of free surface charge and the surface current density vanish. The boundary conditions can be then expressed in a compact matrix form using co called dynamical matrices $\mathbf{D}_i$ coupling the mentioned tangential field components to wave amplitudes on the boundaries. The propagation through i-th layer is described using propagation matrices $\mathbf{P}_i$ [25]. In order to obtain the complex reflection/transmission coefficients describing the reflection or transmission properties of the whole structure, one can consider the complex amplitudes U of incident (I), reflected (R), transmitted (T) and backward incident (B) waves, which are coupled by a total transmission matrix $\mathbf{M}$ of the structure:

$$\begin{bmatrix} U_{\mathrm{R}}^{(0)} \\ U_{\mathrm{I}}^{(0)} \end{bmatrix} = \begin{bmatrix} M_{11} & M_{12} \\ M_{21} & M_{22} \end{bmatrix} \begin{bmatrix} U_{\mathrm{T}}^{(N+1)} \\ U_{\mathrm{B}}^{(N+1)} \end{bmatrix} \quad \text{where} \quad \mathbf{M} = \mathbf{D}_0^{-1} \left[\prod_{i=1}^{N} \mathbf{D}_i \mathbf{P}_i \mathbf{D}_i^{-1} \right] \mathbf{D}_{N+1} \,. \tag{5}$$

Here N is the number of layers, and indices 0 and $N + 1$ refer to the first and last semi-infinite media.

In our case all media are isotropic, so we have 2×2 matrices and s and p polarizations can be treated separately (for details about matrix elements see [25]). Usually there is not backward incident wave, so $U_{\mathrm{B}} = 0$ and the required complex refection/transmission coefficients are expressed using total transmission matrix elements:

$$r = \left(\frac{U_{\mathrm{R}}^{(0)}}{U_{\mathrm{I}}^{(0)}} \right)_{U_{\mathrm{B}}^{(N+1)}=0} = \frac{M_{21}}{M_{11}} \qquad \text{and} \qquad t = \left(\frac{U_{\mathrm{T}}^{(N+1)}}{U_{\mathrm{I}}^{(0)}} \right)_{U_{\mathrm{B}}^{(N+1)}=0} = \frac{1}{M_{11}} \,. \tag{6}$$

In our model the SPR structure consists of three layers: chromium adhesion layer and two layers representing the real gold layer - the homogeneous Au layer is followed by effective media layer representing surface roughness. So we decided to use the above described matrix formalism, and computed the required complex reflection coefficient r for both s and p polarizations using Eqs. (5) and (6).

The material dispersion characteristics of all media have to be included into a computation procedure, as the measurements are performed in the spectral domain. The dispersion of the coupling prism and glass plate (both made from SF10 glass) are well described by a three-oscillator Sellmeier equation [26]. Because the glass refractive index is a temperature sensitive quantity, this feature was taken into account too (for details see [27]). The dispersion of adhesion Cr layer was described using a Kramers-Kronig consistent formula derived using critical points theory [28], and the dispersion of surrounding air was modeled using a two-term Sellmeier-like equation including the influence of temperature [29]. As the spectral dependence of the complex permittivity of gold is the subject of the presented study, this topic is addressed in details in the following text.

To describe the complex permittivity of gold as a function of wavelength, models such as the Drude-Lorentz model, a combination of Drude and critical points models [17, 28, 30] and a modified Drude-Lorentz model [31] can be adopted. The models describe the dispersion in the considered spectral region with different accuracy dependent on the number of parameters

Optical Materials EXPRESS

used. We prefer to use the Drude-Lorentz model with two additional Lorentzian terms [30, 31] which proved to be effective in our previous works [22, 24]. The wavelength dependence of the complex permittivity of gold is expressed as follows

$$\varepsilon_{\mathrm{Au}}(\lambda) = 1 - \frac{1}{\lambda_p^2(1/\lambda^2 + i/\gamma_p\lambda)} - \sum_{j=1}^{2} \frac{A_j}{\lambda_j^2(1/\lambda^2 - 1/\lambda_j^2) + i\lambda_j^2/\gamma_j\lambda}, \tag{7}$$

where parameters λ_p, γ_p, A_j, λ_j, and γ_j are specified in [24].

4. Experimental results and discussion

A gold film under study is related to a sample with no history. Measurements of the phase shifts $\delta(\lambda)$ for different angles of incidence α were performed after the reference measurement that enables the reference phase difference $\Delta_{\mathrm{ref}}(\lambda)$ to be determined. The reference measurement was performed for the SF10 prism alone and the angle of incidence α on the prism face was adjusted to be 0° so that the angle of incidence θ on the base of the equilateral prism was 60°. An example of the recorded reference channeled spectrum is shown in Fig. 2(a) and it is clearly seen that the spectral interference fringes of a sufficient visibility are resolved in the considered spectral range. In the same figure is also shown the channeled spectrum for the SPR structure when the angle of incidence α on the prism face was adjusted to be 40°. The outer medium is air and the SPR phenomenon is pronounced by the visibility decrease and abrupt phase shift near the resonance wavelength.

The phase shift $\delta(\lambda)$ defined by Eq. (4) can be obtained by processing both channeled spectra using a windowed Fourier transform [32] and the result is shown in Fig. 2(b). It is evident that the SPR is manifested as an abrupt phase change with respect to the reference phase for the interference resolved with the SF10 glass prism alone. The derivative of the phase shift is with maximum to which a resonance wavelength of 606.35 nm corresponds.

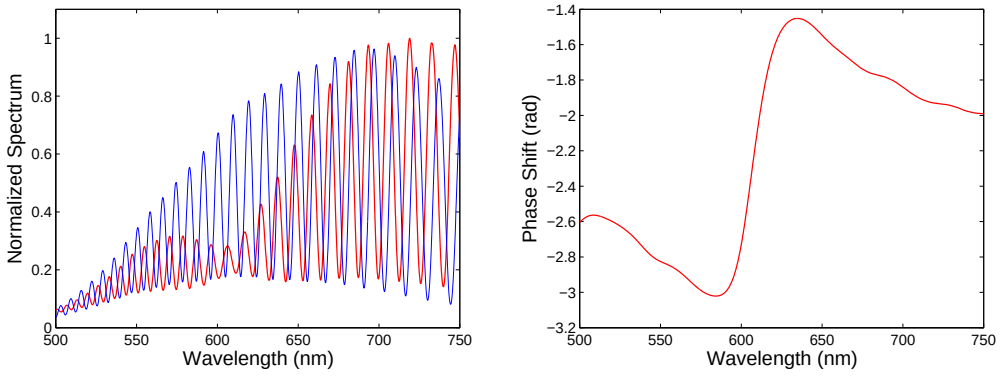

(**a**) (**b**)

Fig. 2. Recorded channeled spectra including (with the visibility decrease) and not including the SPR effect (a). The corresponding phase shift $\delta(\lambda)$ as a function of wavelength λ (b).

Next, other 34 values of angle of incidence α were adjusted in a desirable range when the SPR phenomenon occurs for air. The angle of incidence was changed using the rotary stage with arm carrying a collimator. The reference angle of incidence, which corresponds to the light beam incident perpendicularly to the prism face, is adjusted to be $\alpha = 0°$. Figure 3(a) shows the measured phase shift $\delta(\lambda)$ as a function of wavelength λ for angle α ranging from 33° to 41°, when steps were 1°, 0.5°and 0.2°, respectively. The phase shifts have abrupt phase changes with amplitudes increasing with increasing angle of incidence. In addition, the slope of the

Optical Materials EXPRESS

phase change near the resonance is increasing with angle of incidence. Similarly, in Fig. 3(b) is shown the measured phase shift $\delta(\lambda)$ as a function of wavelength λ for angle of incidence ranging from 41.1° to 42.6° with a step of 0.1°. For these angles of incidence, amplitudes of the abrupt phase changes are decreasing and the resonance wavelength shifts toward longer wavelengths as the angle of incidence increases. Moreover, the slope of the phase change near the resonance decreases with increasing angle of incidence.

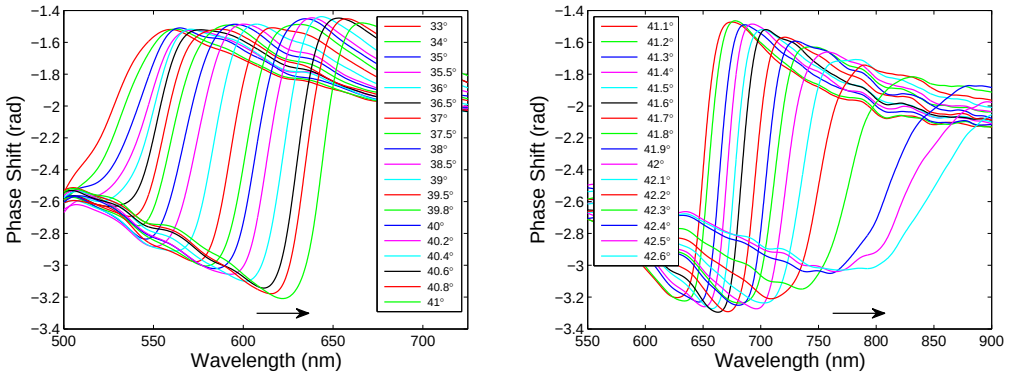

(**a**) (**b**)

Fig. 3. Measured phase shift $\delta(\lambda)$ as a function of the wavelength λ for different angles of incidence α: 33° to 41° (a), 41.1° to 42.6° (b).

The abrupt phase changes near resonance are manifested by peaks of the phase shift derivatives $\mathrm{d}\delta(\lambda)/\mathrm{d}\lambda$ shown as a function of wavelength λ in Fig. 4(a) for angle α ranging from 33° to 41°. The resonance wavelength, which is given by a wavelength of maximum in the phase shift derivative $\mathrm{d}\delta(\lambda)/\mathrm{d}\lambda$, increases as the angle of incidence increases. In addition, the resonance peak increases and narrows with increasing angle of incidence, what means that the slope in the phase function $\delta(\lambda)$ is higher, and the resolution of the maximum position is better. In contrary, the phase shift derivatives $\mathrm{d}\delta(\lambda)/\mathrm{d}\lambda$ shown in Fig. 4(b) for angle α ranging from 41.1° to 42.6° have the resonance peaks that decrease and widen with increasing angle of incidence, what means that the slope in the phase function $\delta(\lambda)$ is smaller, and the resolution of the maximum position is worse.

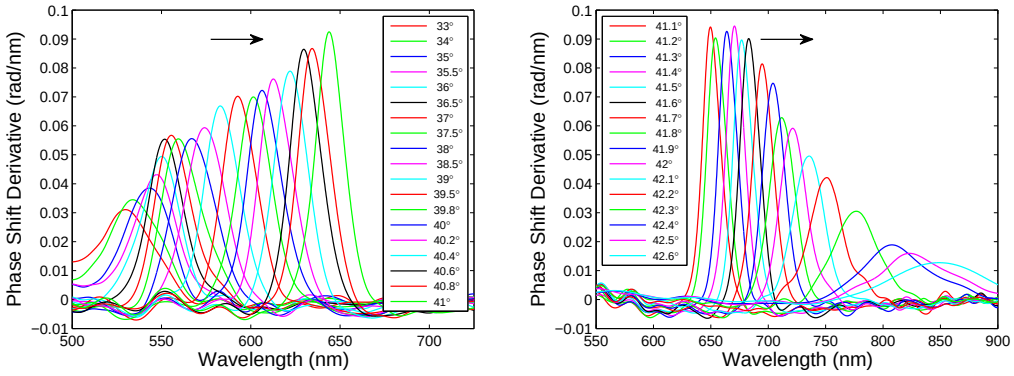

(**a**) (**b**)

Fig. 4. Measured phase shift derivative $\mathrm{d}\delta(\lambda)/\mathrm{d}\lambda$ as a function of the wavelength λ for different angles of incidence α: 33° to 41° (a), 41.1° to 42.6° (b).

Optical Materials EXPRESS

To determine the wavelength dependence of the complex permittivity of a thin gold film under study from the measured wavelength dependencies of the phase shift $\delta(\lambda)$, we adopt an approach which is similar to that used in our previous work [22]. In this approach, the complex permittivity function of a thin gold film is expressed according to a proposed physical model, namely a modified Drude-Lorentz model given by Eq. (7). Then the measured phase shifts $\delta(\lambda)$ for different angles of incidence are processed to obtain the corresponding complex permittivity as a function of the resonance wavelength. Using the individual values of the complex permittivity thus obtained in a whole measured wavelength range, they are fitted to a model function according to Eq. (7) and their parameters λ_p, γ_p, A_j, λ_j, and γ_j are determined.

To illustrate the processing procedure, in Fig. 5(a) is shown by the dashed curve the result for the phase shift $\delta(\lambda)$ measured at an angle of incidence of 40°. In the processing procedure, the measured phase shift $\delta(\lambda)$ was fitted within a 100 nm wavelength range around a resonance wavelength of 606.35 nm. The starting parameters λ_p, γ_p, A_j, λ_j, and γ_j in the modified Drude-Lorentz model according to Eq. (7) were taken from [24] and the values of the real and imaginary permittivity at a resonance wavelength of 606.35 nm thus obtained are -10.261 and 1.762, respectively. It is clearly seen that both curves in the fit agree well and the difference between them is only in a long wavelength range. Consequently, the approach is also supported by the phase shift derivative $\mathrm{d}\delta(\lambda)/\mathrm{d}\lambda$ shown in Fig 5(b). Once again, both curves agree well and the differences between them are on the wings of the resonance peak.

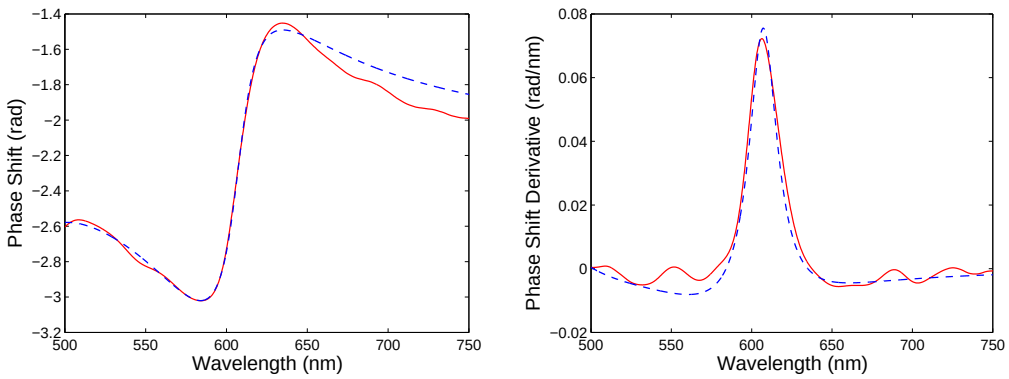

(**a**) (**b**)

Fig. 5. Measured phase shift $\delta(\lambda)$ (a) and its derivative $\mathrm{d}\delta(\lambda)/\mathrm{d}\lambda$ (b) as a function of the wavelength λ (solid curves) for angle of incidence $\alpha = 40°$ together with the the results of the fit (dashed curves).

Similar approach was applied to the remaining measured wavelength dependencies of the phase shift $\delta(\lambda)$ shown in Figs. 3(a) and 3(b), and the corresponding values of real and imaginary permittivity were determined at the resonance wavelengths, given by the positions of maxima of the phase shift derivative $\mathrm{d}\delta(\lambda)/\mathrm{d}\lambda$ shown in Figs. 4(a) and 4(b). Next, Fig. 6(a) shows the wavelength dependence of the real part of the permittivity thus obtained. A fit according to the model function given by Eq. (7) is shown by a solid line, and also the real permittivity function corresponding to a model with parameters from [24] is included. Similarly, Fig. 6(b) shows the wavelength dependence of the imaginary part of the permittivity. Once again, a fit and the reference function are shown. In the same figures are shown by dashed lines the results of the polarimetry measurements [22]. They agree very well in the real part of the permittivity, but differ in the imaginary part. This due to the fact that the imaginary part of the permittivity is dependent on the reflectance ratio at the resonance wavelength and thus, it is very sensitive to a read optical fiber used in the polarimetry measurements.

Optical Materials EXPRESS

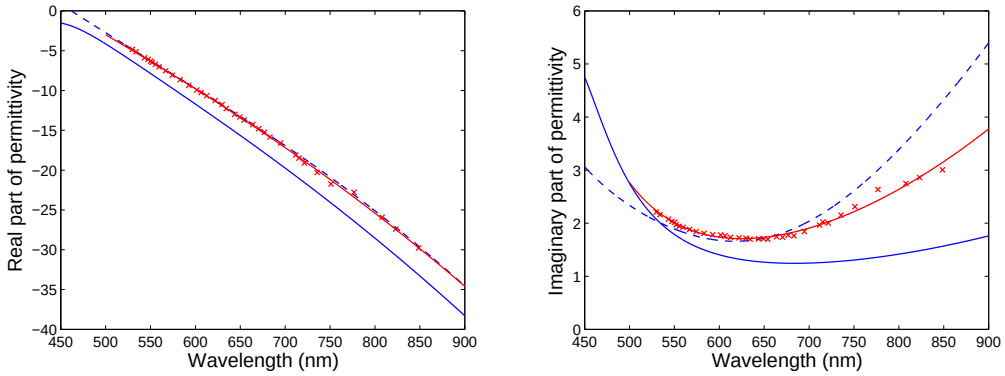

(**a**) (**b**)

Fig. 6. Complex permittivity of the gold film (crosses) as a function of the wavelength with a fit according to a modified Drude-Lorentz model: a real part (a), an imaginary part (b). Dashed lines are the results of the polarimetry measurements [22] and lower curves correspond to a model permittivity (7) with parameters from [24].

Generally, taking into account the fact that a wavelength uncertainty with which the channeled spectra are recorded is 0.2 nm, the errors of the real and imaginary permittivity can be specified [22]. As an example, at a resonance wavelength of 606.35 nm, the errors are ±0.014 and ±0.001, respectively. In addition, these errors increase with increasing wavelength. Similarly, taking into account the fact that an angle uncertainty with which the angle of incidence is adjusted is ±0.01°, a resonance wavelength of 606.35 nm is with error ±0.28 nm, so that the errors of the real and imaginary permittivity are ±0.020 and ±0.001, respectively. Once again, these errors increase with increasing wavelength.

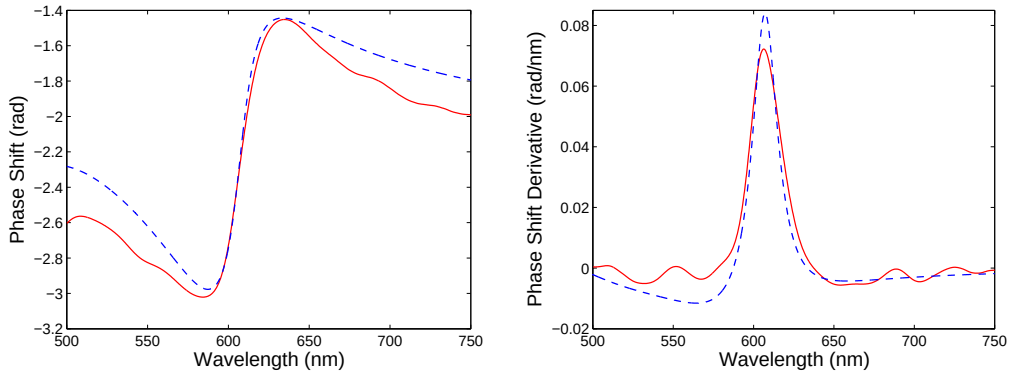

(**a**) (**b**)

Fig. 7. Measured phase shift $\delta(\lambda)$ (a) and its derivative $\mathrm{d}\delta(\lambda)/\mathrm{d}\lambda$ (b) as a function of the wavelength λ (solid curves) for angle of incidence $\alpha = 40°$ together with the result of the modeling (dashed curves).

The complex permittivity function (7) of the thin gold film under test, parameters of which are specified in Table 1, can be used to model the responses of the SPR structure at different angles of incidence. As an example, Fig. 7(a) shows comparison of the phase shift $\delta(\lambda)$ measured for angle of incidence $\alpha = 40°$ with the modeled one. It is clearly seen that the phase shift function agree well in the vicinity of the resonance wavelength, but the difference between the curves is in both short and long wavelength ranges. Similarly, Fig. 7(b) shows comparison of the phase

Optical Materials EXPRESS

shift derivative $d\delta(\lambda)/d\lambda$ with the modeled one. Similarly, the phase shift derivatives agree well regarding the resonance wavelength, but they differ in a short wavelength range.

Table 1. Parameters of dielectric function of Au retrieved from the measurement.

Drude term		Oscillator 1		Oscillator 2	
Parameter	value	Parameter	value	Parameter	value
ε_∞	1	A_1	5.15	A_2	2.96
λ_p(nm)	135.55	λ_1(nm)	344.8	λ_2(nm)	137.91
γ_p(nm)	9235.1	γ_1(nm)	-32.19	γ_2(nm)	-34.61

5. Conclusions

In this paper, a novel phase sensitive technique for measuring the complex permittivity function of a thin gold film was proposed and confirmed. The gold film is part of an SPR structure represented by a gold coated SF10 slide with an adhesion film of chromium attached to an SF10 glass prism. The measurement method, which is based on spectral interferometry and employs a setup with a birefringent crystal and the SPR structure in the Kretschmann configuration, overcomes the disadvantages of a polarimetric method. From the recorded channeled spectra the phase functions of the SPR for air at different angles of incidence are retrieved, and the SPR phenomenon is manifested by an abrupt phase change with respect to the reference phase difference resolved for the interference with the SF10 glass prism alone. These phase changes are processed in the vicinity of the resonance wavelengths to obtain the complex permittivity function which is described by the Drude-Lorentz model with two additional Lorentzian terms. The feasibility of the technique was demonstrated for the thin gold film of known thickness parameters, when the complex permittivity function was measured in a wavelength range from 530 to 850 nm. This phase sensitive method is demonstrated to be effective in measuring the complex permittivity function of thin metal films of SPR structures, directly in the Kretschmann configuration.

Funding

ERDF/ESF project New Composite Materials for Environmental Applications (No. CZ.02.1.01/0.0/0.0/17_048/0007399).

References

1. J. M. Pitarke, V. M. Silkin, E. V. Chulkov, and P. M. Echenique, "Theory of surface plasmons and surface-plasmon polaritons," Rep. Prog. Phys. **70**, 1–87 (2007).
2. E. Kretschmann and H. Raether, "Radiative decay of nonradiative surface plasmons excited by light," Z. Naturforschung **A23**, 2135–2136 (1968).
3. A. Otto, "Excitation of nonradiative surface plasma waves in silver by the method of frustrated total reflection," Z. für Physik **216**, 398–410 (1968).
4. H. Raether, *Surface Plasmons on Smooth and Rough Surfaces and on Gratings* (Springer-Verlag, New York, 1988).
5. M. Manuel, B. Vidal, R. Lopéz, S. Alegret, J. Alonso-Chamarro, I. Garces, and J. Mateo, "Determination of probable alcohol yield in musts by means of an SPR optical sensor," Sens. Actuators B **11**, 455–459 (1993).
6. J. Homola, *Surface Plasmon Resonance Based Sensors* (Springer-Verlag, New York, 2006).
7. P. Nikitin, A. Beloglazov, V. Kochergin, M. Valeiko, and T. Ksenevich, "Surface plasmon resonance interferometry for biological and chemical sensing," Sens. Actuators B **54**, 43–50 (1999).

Optical Materials EXPRESS

8. B. Liedberg, C. Nylander, and I. Lundström, "Principles of biosensing with an extended coupling matrix and surface plasmon resonance," Sens. Actuators B **11**, 63–72 (1993).
9. J. Dostálek, H. Vaisocherova, and J. Homola, "Multichannel surface plasmon resonance biosensor with wavelength division multiplexing," Sens. Actuators B **108**, 758–764 (2005).
10. H. R. Gwon and S. H. Lee, "Spectral and angular responses of surface plasmon resonance based on the Kretschmann prism configuration," Mater. Trans. **51**, 1150–1155 (2010).
11. S. H. El-Gohary, M. Choi, Y. L. Kim, and K. M. Byun, "Dispersion curve engineering of TiO2/silver hybrid substrates for enhanced surface plasmon resonance detection," Sensors **16**, 1442 (2016).
12. A. Shalabney and I. Abdulhalim, "Figure-of-merit enhancement of surface plasmon resonance sensors in the spectral interrogation," Opt. Lett. **37**, 1175–1177 (2012).
13. P. Hlubina, M. Duliakova, M. Kadulova, and D. Ciprian, "Spectral interferometry-based surface plasmon resonance sensor," Opt. Commun. **354**, 240–245 (2015).
14. S.-G. Huang, K.-P. Chen, and S.-C. Jeng, "Phase sensitive sensor on Tamm plasmon devices," Opt. Mater. Express **4**, 1267–1273 (2017).
15. H. Fujiwara, *Spectroscopic Ellipsometry: Principles and Applications* (John Wiley and Sons Ltd., Chichester, 2007).
16. M. Y. Zhang, Z. Y. Wang, T. N. Zhang, Y. Zhang, R. J. Zhang, X. Chen, Y. Sun, Y. X. Zheng, S. Y. Wang, and L. Y. Chen, "Thickness-dependent free-electron relaxation time of au thin films in near-infrared region," J. Nanophoton. **516**, 033009 (2016).
17. E. T. Hu, Q. Y. Cai, R. J. Zhang, Y. F. Wei, W. C. Zhou, S. Y. Wang, Y. X. Zheng, W. Wei, and L. Y. Chen, "Effective method to study the thickness-dependent dielectric functions of nanometal thin film," Opt. Lett. **41**, 4907–4910 (2016).
18. X. Sun, R. Hong, H. Hou, Z. Fan, and J. Shao, "Thickness dependence of structure and optical properties of silver films deposited by magnetron sputtering," Thin Solid Films **515**, 6962–6966 (2007).
19. G. Hu, H. He, A. Sytchkova, J. Zhao, J. Shao, M.Grilli, and A. Piegari, "High-precision measurement of optical constants of ultra-thin coating using surface plasmon resonance spectroscopic ellipsometry in Otto-Bliokh configuration," Opt. Express **25**, 13425–13434 (2017).
20. Z. M. Qi, M. Wei, H. Matsuda, I. Honma, and H. Zhou, "Broadband surface plasmon resonance spectroscopy for determination of refractive index dispersion of dielectric thin films," Appl. Phys. Lett. **90**, 181112 (2007).
21. H. Yan, Y. Hong-An, L. Song-Quan, and D. Yin-Feng, "The determination of the thickness and the optical dispersion property of gold film using spectroscopy of a surface plasmon in the frequency domain," Chin. Phys. B **22**, 027301 (2013).
22. R. Chlebus, J. Chylek, D. Ciprian, and P. Hlubina, "Surface plasmon resonance based measurement of the dielectric function of a thin metal film," Sensors **18**, 3693 (2018).
23. P. Hlubina, J. Luňáček, and D. Ciprian, "Spectral interferometric technique to measure ellipsometric phase of a thin-film structure," Opt. Lett. **34**, 2661–2663 (2009).
24. P. Hlubina and D. Ciprian, "Spectral phase shift of surface plasmon resonance in the Kretschmann configuration: theory and experiment," Plasmonics **12**, 1071–1078 (2017).
25. P. Yeh, *Optical Waves in Layered Media* (J. Wiley and Sons, Inc., New York, 1988).
26. "Schott technical information, TIE-29: Refractive index and dispersion," https://www.us.schott.com.
27. "Schott technical information, TIE-29: Temperature coefficient of the refractive index," https://www.us.schott.com.
28. A. Vial and T. Laroche, "Description of dispersion properties of metals by means of the critical points model and application to the study of resonant structures using the FDTD method," J. Phys. D: Appl. Phys. **40**, 7152–7158 (2007).
29. H. Bach and N. Neuroth, *eds., The Properties of Optical Glass* (Springer-Verlag, Berlin, Heidelberg, 1998).
30. A. Vial, A.-S. Grimault, D. Macías, D. Barchiesi, and M. L. de la Chapelle, "Improved analytical fit of gold dispersion: Application to the modeling of extinction spectra with a finite-difference time-domain method," Phys. Rev. B **71**, 085416 (2005).
31. Z. Yang, D. Gu, and Y. Gao, "An improved dispersion law of thin metal film and application to the study of surface plasmon resonance phenomenon," Opt. Commun. **329**, 180–183 (2014).
32. P. Hlubina, J. Luňáček, D. Ciprian, and R. Chlebus, "Windowed Fourier transform applied in the wavelength domain to process the spectral interference signals," Opt. Commun. **281**, 2349–2354 (2008).